RSC Advances

PAPER

View Article Online
View Journal | View Issue

Cite this: *RSC Adv.*, 2014, **4**, 28908

Pt-doped graphene oxide/MIL-101 nanocomposites exhibiting enhanced hydrogen uptake at ambient temperature†

Jun Zhang,[a] Xiaoqing Liu,[b] Hu Zhou,[bc] Xiufen Yan,[a] Yuanjun Liu[a] and Aihua Yuan*[a]

Received 21st February 2014
Accepted 18th June 2014

DOI: 10.1039/c4ra01540a

www.rsc.org/advances

Nanocomposites of Pt-doped graphene oxide (GO) and a chromate–organic framework (MIL-101) were prepared through the *in situ* solvent-thermal method. The parent materials and all composites have been characterized by powder X-ray diffraction, scanning electron microscopy, transmission electron microscopy, energy dispersive spectroscopy, and gas adsorption analysis. The results indicated that the incorporation of a Pt/GO component did not prevent the formation of MIL-101 units. However, the crystallinities, morphologies, and surface areas of the composites were affected obviously by the Pt/GO content. The significant enhancement by a factor of 1.57–2.69 of hydrogen storage capacities at ambient temperature and 10 bar for the composites can be attributed reasonably to the spillover mechanism in such a system, in which Pt nanoparticles act as the spillover source of hydrogen molecules, while GO and MIL-101 act as the primary and secondary receptors, respectively.

1. Introduction

Metal–organic frameworks (MOFs) have received tremendous attention for the potential application in the field of hydrogen storage, due to their large surface areas, high porosities, and adjustable pore sizes.[1] However, the high hydrogen storage capacities of current MOFs were measured only at 77 K and decreased dramatically at ambient temperature. This can be reasonably ascribed to the very weak van der Waals interactions between hydrogen molecules and MOFs. For example, the hydrogen uptake for MIL-101 is below 0.4 wt% at 298 K and 65 bar, although this material has a very high Langmuir surface area of 5900 $m^2\ g^{-1}$ and hydrogen adsorption amount of 6.1 wt% at 77 K and 80 bar.[2,3]

Recently, the hydrogen storage capacities of sorbents have been increased significantly by the spillover technique.[4,5] Hydrogen spillover is generally defined as the hydrogen molecules dissociation and chemisorption on transition metal nanoparticles, followed by migration of atomic hydrogen onto adjacent receptor surfaces *via* spillover and surface diffusion.[6–8] Yang and coworkers have demonstrated that obviously enhanced hydrogen uptakes were achieved by mixing physically a small quantity of Pt/AC catalysts with the MOF receptors and then building carbon bridges between them, in which the measured hydrogen storage capacities of IRMOF-8 and IRMOF-1 were close to 4.0 and 3.0 wt% (100 bar, 298 K), respectively.[9,10] Similarly, mixing mechanically MIL-101 with Pt/C catalysts also improved the hydrogen storage capacity from 0.54 wt% to 0.75 wt% at 293 K and 50 bar, with a further increase to 1.14 wt% after the bridging treatment.[11] Unfortunately, the reproducibility of hydrogen spillover enhancement by the physically mixing and bridge-building method was affected by many experimental factors during materials preparation.[12–14] To maximize the spillover effect was highly empirical and difficult to achieve.

Graphene oxide (GO) is very suitable to construct graphene-based composites because of their rich functional oxygen groups on the surface and edge.[15] GO/MOF hybrid composites have been synthesized recently through the reaction between GO and precursors of MOF, and the synergetic effect between two components was responsible for enhanced adsorption amounts of gases (N_2, NH_3, H_2S, NO_2, CO_2) compared to the pure MOF.[16–19]

Combining the merits of the spillover mechanism and GO/MOF composites, series of Pt@GO/HKUST-1 nanocomposites have been documented recently by our group through the *in situ* synthesis method, which represent the first samples of Pt-doped GO/MOF hybrid system.[20] Direct *in situ* incorporation of Pt/GO catalysts into MOF units exhibited more controllable and reproducible. In addition, the spillover mechanism and the synergetic effect of different components have resulted in the

[a]*School of Biology and Chemical Engineering, Jiangsu University of Science and Technology, Zhenjiang 212003, P. R. China. E-mail: aihua.yuan@just.edu.cn; Fax: +86 511 85635850; Tel: +86 511 85638920*

[b]*School of Material Science and Engineering, Jiangsu University of Science and Technology, Zhenjiang 212003, P. R. China*

[c]*SiYang Diesel Engine Manufacturing Co., Ltd, Zhenjiang 212003, P. R. China*

† Electronic supplementary information (ESI) available: XRD patterns, element mapping images, and low-pressure hydrogen adsorption isotherms at 298 K and 77 K. See DOI: 10.1039/c4ra01540a

significant enhancement of hydrogen storage capacities at ambient temperature. This result inspires our group to further investigate the structure–properties correlations and the spill-over phenomenon for the Pt-doped GO/MOF system.

MIL-101, as a very prominent adsorbent among MOFs, is constructed from benzene-1,4-dicarboxylate and trimetric chromium(III) octahedral cluster,[2] and its adsorption properties have been studied extensively. Recently, the GO/MIL-101 composites have been synthesized successfully and adsorption capacities of composites for *n*-hexane and acetone were higher than those of the parent material MIL-101.[21,22] This enhancement can be reasonably attributed to the increase in the specific surface areas of composites and the dispersive forces due to the introduction of GO component. In the previous studies, Bandosz and coworkers have compared in detail the structural chemistry and adsorption properties of the GO/MOF system constructed by different types of MOFs (MOF-5, HKUST-1 or MIL-100(Fe)) and GO.[18] The results showed that the diversity of structure and coordination mode affected obviously the formation and adsorption properties of composites. As we all known, MIL-101 has spherical pores, and a distinctly different structure and coordination mode compared to HKUST-1 and MOF-5. So, as a part of a detailed study of Pt-doped GO/MOF system, our further effort is to prepare the new composite using MIL-101 as the component and to highlight characteristic features of the MOF chemistry for both the formation of composites and hydrogen adsorptions at ambient temperature. The present contribution focused on the syntheses, characterizations, and hydrogen adsorption properties at room temperature of Pt-doped GO/MIL-101 composites, by the self-assembly reaction between Pt/GO catalysts and precursors of MIL-101.

2. Experimental

2.1. Materials and physical measurements

Unless otherwise mentioned, all reactants were used as purchased without further purification. Powder X-ray diffraction (XRD) measurements were carried out using a Shimadzu XRD-6000 diffractometer with CuK_α ($\lambda = 0.1543$ nm) radiation. IR spectra were measured on a Nicolet FT 1703X spectrophotometer in the 4000–400 cm^{-1} region (KBr pellets). The morphologies and structures of the samples were determined by the scanning electron microscope (SEM, JEOL JSM-6480) and transmission electron microscopy (TEM, JEOL JEM-2100). The compositions of materials were examined by energy-dispersive X-ray spectrometry (EDS, Oxford INCA). Nitrogen and low-pressure hydrogen adsorption isotherms were performed using the accelerated surface area and porosimetry analyzer (Micromeritics, ASAP 2020). High-pressure hydrogen uptakes were investigated on ASAP 2050 volumetric instruments (Micromeritics). Prior to experiments, all samples were outgassed at 180 °C for 24 h. UHP grade N_2 and H_2 (99.999%) gases were used for all measurements. The BET specific surface area was calculated using adsorption data in the relative pressure range of 0.06–0.30. The pore volume was calculated by a single point method at $P/P_0 = 0.99$.

2.2. Syntheses

2.2.1. Preparation of Pt-doped graphene oxide. Graphene oxide (GO) was prepared according to a modified Hummers method.[23] Pt particles were introduced onto the GO surface using a chemical reduction method.[24] Briefly, GO (50 mg) was dispersed in deionized (DI) water (50 mL) by sonication for 30 min, forming the stable GO colloid. The ethylene glycol (100 mL) and DI water solution (2.5 mL) of $H_2PtCl_6 \cdot 6H_2O$ (0.01 M) were added to the solution with magnetic stirring for 30 min. Subsequently, the mixture was put in an oil bath and heated at 100 °C for 6 h under stirring. The products were separated from the ethylene glycol solution in the centrifuge, washed with DI water, and dried in an oven at 60 °C overnight. The final product was referred as PG.

2.2.2. Preparation of MIL-101. MIL-101 was prepared according to the published procedure.[2] 1,4-Benzene dicarboxylic acid (H_2BDC) (164 mg, 1 mmol), $Cr(NO_3)_3 \cdot 9H_2O$ (400 mg, 1 mmol), fluorhydric acid (HF) (1 mmol), and 4.8 mL H_2O (265 mmol) were mixed and sealed in a Teflon lined hydrothermal autoclave. The mixture was heated at 220 °C for 8 hours and cool down slowly to room temperature, producing crystallized powders. The powders were filtered and washed with distilled water and refluxed in NH_4F to remove the unreacted BDC molecules present as needles after synthesis. The resulting products were dried overnight at 60 °C.

2.2.3. Preparation of Pt-doped GO/MIL-101 composites. The composites were prepared in the same procedure as MIL-101 except that various amounts of PG were added to the mixture of MIL-101 precursors upon sonication before the heat treatment. The added GO consisted of 2, 5, and 10 wt% of the final material weight. The composites are referred as MPG2, MPG5 and MPG10, respectively.

3. Results and discussion

3.1. Powder XRD patterns

The crystallinities of the parent components and composites were investigated by powder XRD patterns. The diffraction peaks for PG can be assigned to the characteristic crystalline

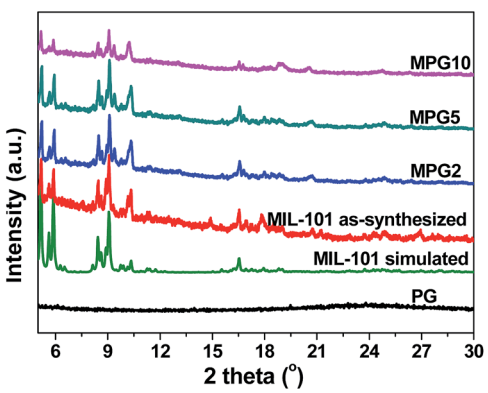

Fig. 1 Powder XRD patterns of the parent materials and composites, compared with those simulated from single-crystal diffraction data of MIL-101.[25]

planes of face-centered-cubic Pt (Fig. S1, ESI†). As shown in Fig. 1, the diffraction peaks of the mesoporous MIL-101 are observed in a small angle region and match well with the already published XRD patterns simulated from single-crystal diffraction data of the same MOF.[25] For the MPG2 and MPG5 composites, the XRD peaks from the parent MIL-101 are mainly preserved, indicating that the incorporation of PG did not disturb or destroy the crystal structure of MOF. It is noticeable that the diffraction intensities for the MPG10 composite decreased significantly, although the diffraction patterns from MIL-101 are mainly preserved in this case. This is related to the low crystallization caused by excessive PG components. No characteristic peaks of PG are detected in the XRD patterns for the three composites, due to the low PG content in composites, or/and the exfoliation/high dispersion of GO in solution upon sonication during the preparation of samples.[24] In fact, the absence of XRD patterns for GO component has also been found in the MOF/GO composites.[16,19,26,27]

3.2. IR spectra

IR spectra of the parent materials and composites were shown in Fig. 2. IR spectrum of PG has been described in detail elsewhere and the vibration peaks of our case are consistent with fingerprint groups.[28] The absorption band at around 1700 cm^{-1} is ascribed to carboxyl groups.[29] The vibration bands related to functional groups of PG are not seen in composites, due to the rather weak adsorption peaks and the low PG content. IR spectra of the parent MIL-101 and the composites exhibit identical bands originating from the carboxylate groups vibrations, characteristic features of such MOF.[2] The symmetric and asymmetric stretching vibrations of carboxylate groups of BDC appear at 1300–1700 cm^{-1}, while the lower wavenumber region of 1300–700 cm^{-1} exhibits various bands assigned to out-of-plane vibrations of BDC. Above analysis is indicative of the coordination of BDC to the chromate(III) centers, and the incorporation of PG did not prevent obviously the formation of MIL-101 units. This supported the results draw from powder XRD experiments and indicates the existence of MOF units in the composites.

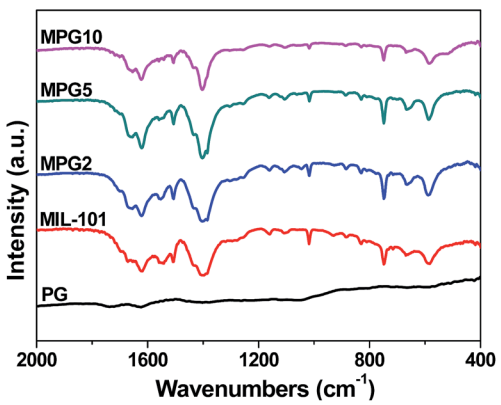

Fig. 2 IR spectra of the parent materials and composites in the region of 4000–400 cm^{-1}.

3.3. Morphologies

The existence of the PG component has caused visible colour change of samples (Fig. S2†). The colour of composites changed much darker green than the parent MIL-101 with the increasing of PG content, indicating the better incorporation of PG into MOF.

SEM and TEM observations were used to investigate the structural details of materials. GO was seen as dense agglomerates of sheets stacked together by dispersive forces (Fig. 3a). It can be seen from TEM images of PG that Pt nanoparticles are densely and uniformly distributed on the surfaces of GO (Fig. 3b). The mean size of Pt particles is approximately 3.5 nm. EDS results of PG further confirm the presence of homogeneously dispersed Pt nanoparticles through GO sheets and the Pt content in PG is about 18.9 wt% (Fig. S3†). The pristine MIL-101 shows well-defined octahedral crystalline shapes (Fig. 4a, 3c), while the composites exhibit some variations caused by the introduction of PG component. The shape of MOF crystals for the MPG2 composite is less regular than that of MIL-101 (Fig. 4b), which may be attributed to a higher degree of defects with the incorporation of PG. The feature is much more pronounced for MPG5 upon increasing the PG content (Fig. 4c). Notably, the presence of smaller particles with a more irregular texture observed for MPG10 (Fig. 4d) suggests the low crystallization of the products. This result has been confirmed by XRD analysis, in which weak diffraction peaks were observed in

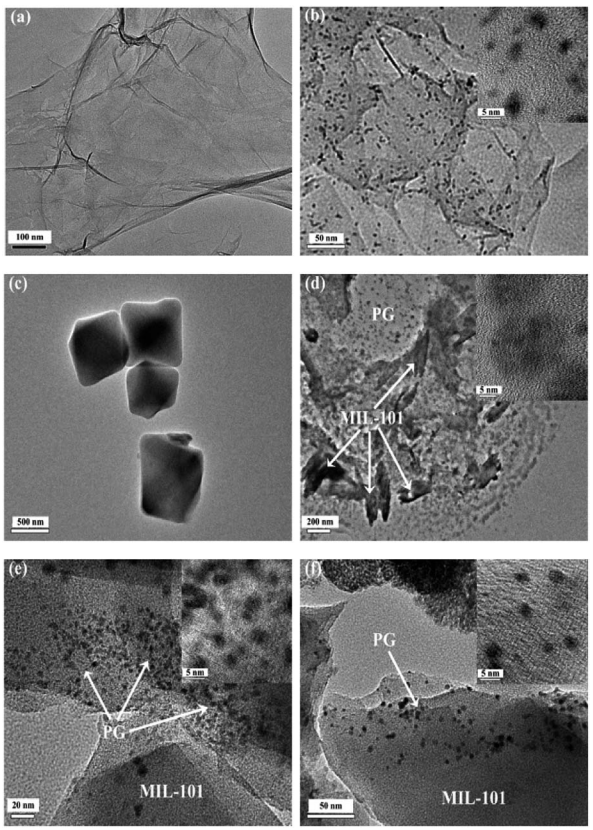

Fig. 3 TEM images of (a) GO, (b) PG, (c) MIL-101, (d) MPG2, (e) MPG5, and (f) MPG10.

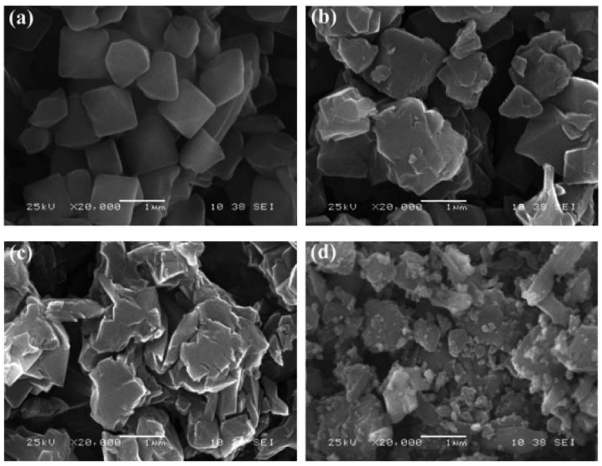

Fig. 4 SEM images of (a) MIL-101, (b) MPG2, (c) MPG5, and (d) MPG10.

MPG10. Practically, the GO layers in our composites have flexible coordination modes with MIL-101 because of the spherical shape of the pores. So the various attachments between oxygen groups of excessive GO layers and Cr(III) sites of MIL-101 prevents the proper building of some MOF units. This formation mechanism has also been found in GO/MIL-100(Fe) materials,[27] but different from that observed in Pt@GO/HKUST-1 composites.[20]

TEM images of composites reveal that Pt particles are dispersed in composites with the micro/nano region (Fig. 3d–f). The increase of PG component in composites has been evidenced by the EDS results (Fig. S4–S7†), in which the percentage of Pt increased gradually from 0.55 wt% in MPG2 to 1.86 wt% in MPG10 *via* 0.69 wt% in MPG5. Simultaneously, the C, O, Cr and Pt are well dispersed in the composites, suggesting that PG and MOF components are mixed throughout the whole samples.

3.4. Textures

The structural difference between MIL-101 and composites can also be confirmed by the analysis of nitrogen adsorption isotherms, as shown in Fig. 5. The PG sample is not shown here due to its negligible porosity. The isotherms of pure MIL-101 and composites are of type-I, indicative of the predominant microporous character on the same MOF.[2,30–35] Powder XRD patterns of the activated MIL-101 sample were consistent to those of as-synthesized MIL-101, indicating the sample did not undergo much structural change (Fig. S8†). The difference in the surface area between our case and the same MOF reported in literatures can be related to the way of outgassing during preparation and thus the completeness of solvent removal, and/or the slight degradation of the porous skeleton, which cannot be detected from XRD patterns.[36] It should be noted that the surface areas and pore volumes of composites were found to continuously decrease as the percentage of PG incorporation increases (Table 1). An obvious decrease observed in MPG10 can be attributed to the fact that the porosity of MIL-101 is reduced dramatically by the addition of high-content nonporous PG, as well as the excessive PG caused much low crystallization of products, as evidenced by XRD analysis and morphological observations.

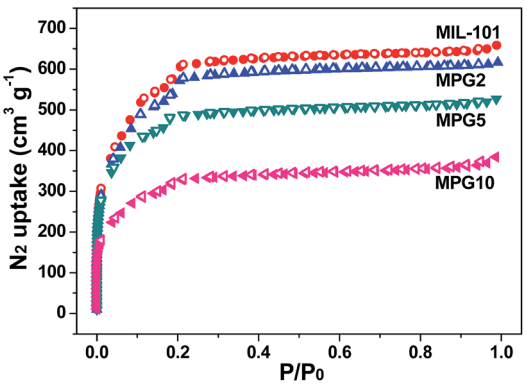

Fig. 5 Nitrogen adsorption isotherms at 77 K of MIL-101 and composites. Filled and hollow symbols indicate the adsorption and desorption branches, respectively.

3.5. Hydrogen storage capacities

High-pressure hydrogen adsorption isotherms of MIL-101 and composites were performed at ambient temperature, as shown in Fig. 6. The hydrogen uptake for the parent MIL-101 at 298 K and 10.0 bar is 12.30 $cm^3\ g^{-1}$ (0.11 wt%), close to that reported in the literature under the similar temperature and pressure condition.[3,11] Surprisingly, the adsorption amounts of the MPG2, MPG5 and MPG10 composites at 298 K and 10.0 bar were 33.09, 30.67 and 19.31 $cm^3\ g^{-1}$, respectively, obviously, the significant enhancement in hydrogen storage capacities at 298 K for all composites could not be ascribed to differences in specific surface area, due to the decreased specific surface area (especially for MPG10) compared to MIL-101.

This phenomenon can be ascribed reasonably to the presence of spillover mechanism involved in such system. In fact, the phenomenon of hydrogen spillover onto MOFs has been reported by several groups through the direct doping of metal nanoparticles,[37–42] physically mixing with Pt/AC or Pt/C catalysts,[9–11,14,43,44] and *in situ* loading of Pt/MWCNTs catalyst.[45] In above systems, the nanoparticles and MOFs act as the spillover source of hydrogen molecules and receptors, respectively. The published reviews have provided tremendous insights into the spillover phenomenon, a detailed investigation into MOFs, and guidance on how to improve hydrogen uptakes of current porous MOFs.[5,46] Also, computational studies have shed light onto the spillover mechanism of MOFs.[47,48] Pt nanoparticles in our composites act as the hydrogen spillover source, and more

Table 1 Parameters of the porous structure derived from the nitrogen isotherms at 77 K for MIL-101 and composites

Samples	S_{BET} ($m^2\ g^{-1}$)	$S_{Langmuir}$ ($m^2\ g^{-1}$)	V_t ($cm^3\ g^{-1}$)
MIL-101	1969	3076	1.02
MPG2	1874	2918	0.95
MPG5	1540	2345	0.82
MPG10	1059	1632	0.59

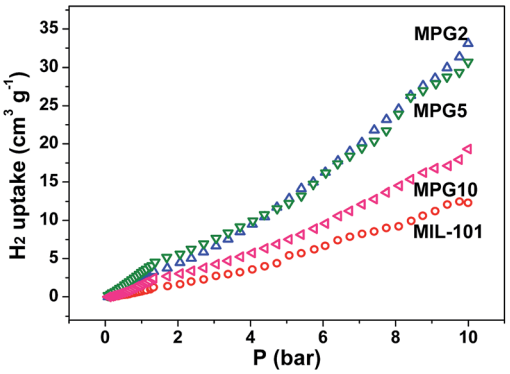

Fig. 6 High-pressure hydrogen adsorption isotherms at 298 K of MIL-101 and composites.

intimate contacts between Pt catalyst and GO/MIL-101 receptor lead to a lower energy barrier for the spillover of dissociated hydrogen from Pt to the receptor, as already observed in Pt/C system.[49] As a result, hydrogen molecules first chemisorbed and dissociated on the surface of Pt and then migrated to the surface of the primary spillover receptor GO. Subsequently, hydrogen atoms further diffuse into the second spillover receptor MIL-101. In fact, the hydrogen spillover was also found in the Pt-doped MWCNTs@MOF-5 hybrid composites, in which the hydrogen storage capacity at 298 K and 100 bar was enhanced 4.2 times higher than that of pure MOF-5 upon the incorporation of Pt/MWCNTs catalyst.[45] The 2.69-, 2.49- and 1.57-fold enhancements for the MPG2, MPG5 and MPG10 composites, respectively, indicate that the spillover mechanism has played an important role in terms of hydrogen storage at ambient temperature. It should be noted that the obvious decrease of hydrogen uptake for MPG10 induced by the low surface area has partially offset the enhancement caused by the spillover effect. However, the measured adsorption capacity for MPG10 was still higher than that observed in MIL-101. Similarly, low-pressure hydrogen adsorption isotherms showed that the MPG2 and MPG5 composites also exhibit higher adsorption capacities than the parent MIL-101 (Fig. S9†), which further confirms the presence of spillover effect in such system. The lower uptake for MPG10 can be ascribed to the fact that the spillover effect was not significant in the low pressure range (0–1 bar) compared to high pressures. The spillover effect at 77 K observed in our composites is not significant compared to that at 298 K (Fig. S10†), which can be reasonably attributed to the low catalytic activity of Pt nanoparticles at extremely low temperatures (*e.g.*, 77 K, 87 K). Similar behaviour has also been observed in the Pt-doped HKUST-1/GO system documented by our group.[20]

4. Conclusions

In summary, series of Pt-doped GO/MIL-101 nanocomposites were synthesized through the *in situ* self-assembly between Pt/GO and precursors of MIL-101. The parent MOF units are mainly preserved in composites, while the crystallinities, morphologies, and texture parameters of composites were induced significantly by the Pt/GO content. In addition, the formation of well-defined Pt-doped GO/MIL-101 composites with high Pt/GO content is not favored because of the specific geometry of MIL-101. The enhancement in hydrogen storage capacities at 298 K for the composites compared to the pristine MOF can be attributed to the spillover effect in such systems. These interesting results provide further insights and understanding of the spillover mechanism for Pt-doped GO/MOF hybrid system. The studies on this line are underway.

Acknowledgements

This research was supported by National Natural Science Foundation (51072072, 51102119, 51272095), Natural Science Foundation of Jiangsu Province (BK2011518), and Qing Lan Project of Jiangsu Province.

Notes and references

1 M. P. Suh, H. J. Park, T. K. Prasad and D. W. Lim, *Chem. Rev.*, 2012, **112**, 782–835.
2 G. Férey, C. Mellot-Draznieks, C. Serre, F. Millange, J. Dutour, S. Surblé and I. Margiolaki, *Science*, 2005, **309**, 2040–2042.
3 M. Latroche, S. Surblé, C. Serre, C. Mellot-Draznieks, P. L. Llewellyn, J. H. Lee, J. S. Chang, S. H. Jhung and G. Férey, *Angew. Chem., Int. Ed.*, 2006, **45**, 8227–8231.
4 L. F. Wang and R. T. Yang, *Catal. Rev.*, 2010, **52**, 411–461.
5 L. F. Wang and R. T. Yang, *Energ. Environ. Sci.*, 2008, **1**, 268–279.
6 A. J. Robell, E. V. Ballou and M. Boudart, *J. Phys. Chem.*, 1964, **68**, 2748–2753.
7 S. T. Srinivas and P. K. Rao, *J. Catal.*, 1994, **148**, 470–477.
8 W. C. Conner and J. L. Falconer, *Chem. Rev.*, 1995, **95**, 759–788.
9 Y. W. Li and R. T. Yang, *J. Am. Chem. Soc.*, 2006, **128**, 726–727.
10 Y. W. Li and R. T. Yang, *J. Am. Chem. Soc.*, 2006, **128**, 8136–8137.
11 Y. Y. Liu, J. L. Zeng, J. Zhang, F. Xu and L. X. Sun, *Int. J. Hydrogen Energy*, 2007, **32**, 4005–4010.
12 S. M. Luzan and A. V. Talyzin, *Microporous Mesoporous Mater.*, 2010, **135**, 201–205.
13 R. Campesi, F. Cuevas, M. Latroche and M. Hirscher, *Phys. Chem. Chem. Phys.*, 2010, **12**, 10457–10459.
14 N. R. Stucket, L. F. Wang and R. T. Yang, *Langmuir*, 2010, **26**, 11963–11971.
15 D. R. Dreyer, S. Park, C. W. Bielawski and R. S. Ruoff, *Chem. Soc. Rev.*, 2010, **39**, 228–240.
16 C. Petit and T. J. Bandosz, *Adv. Mater.*, 2009, **21**, 4753–4757.
17 C. Petit, J. Burress and T. J. Bandosz, *Carbon*, 2011, **49**, 563–572.
18 C. Petit and T. J. Bandosz, *Dalton Trans.*, 2012, **41**, 4027–4035.
19 R. Kumar, K. Jayaramulu, T. K. Maji and C. N. R. Rao, *Chem. Commun.*, 2013, **49**, 4947–4949.

20 H. Zhou, X. Q. Liu, J. Zhang, X. F. Yan, Y. J. Liu and A. H. Yuan, *Int. J. Hydrogen Energy*, 2014, **39**, 2160–2167.
21 S. J. Sun, Q. B. Xia, Z. X. Zhao, Y. W. Li and Z. Li, *Chem. Eng. J.*, 2014, **239**, 226–232.
22 X. Zhou, W. Y. Huang, J. Shi, Z. X. Zhao, Q. B. Xia, Y. W. Li, H. H. Wang and Z. Li, *J. Mater. Chem. A*, 2014, **2**, 4722–4730.
23 W. S. Hummers and R. E. Offeman, *J. Am. Chem. Soc.*, 1958, **80**, 1339.
24 D. Y. Cai and M. Song, *J. Mater. Chem.*, 2007, **17**, 3678–3680.
25 O. L. Lebedev, F. Millange, C. Sere, G. Van Tendelo and G. Férey, *Chem. Mater.*, 2005, **17**, 6525–6527.
26 S. Liu, L. X. Sun, F. Xu, J. Zhang, C. L. Jiao, F. Li, Z. B. Li, S. Wang, Z. Q. Wang, X. Jiang, H. Y. Zhou and L. N. Yang, *Energy Environ. Sci.*, 2013, **6**, 818–823.
27 C. Petit and T. J. Bandosz, *Adv. Funct. Mater.*, 2011, **21**, 2108–2117.
28 C. Xu, X. Wang and J. W. Zhu, *J. Phys. Chem. C*, 2008, **112**, 19841–19845.
29 D. Li, M. B. Müller, S. Gilje, R. B. Kaner and G. G. Wallace, *Nat. Nanotechnol.*, 2008, **3**, 101–105.
30 H. Y. Pan, X. H. Li, D. M. Zhang, Y. J. Guan and P. Wu, *J. Mol. Catal. A: Chem.*, 2013, **377**, 108–114.
31 W. C. Du, G. Z. Chen, R. F. Nie, Y. W. Li and Z. Y. Hou, *Catal. Commun.*, 2013, **41**, 56–59.
32 G. Z. Chen, S. J. Wu, H. L. Liu, H. F. Jiang and Y. W. Li, *Green Chem.*, 2013, **15**, 230–235.
33 K. P. Prasanth, P. Ralapalli, M. C. Raj, H. C. Bajaj and R. V. Jasra, *Int. J. Hydrogen Energy*, 2011, **36**, 7594–7601.
34 Y. W. Li and R. T. Yang, *AIChE J.*, 2008, **54**, 269–279.
35 K. S. Lin, A. K. Adhikari, Y. H. Su, C. W. Shu and H. Y. Chan, *Adsorption*, 2012, **18**, 483–491.
36 S. S. Kaye, A. Dailly, O. M. Yaghi and J. R. Long, *J. Am. Chem. Soc.*, 2007, **129**, 14176–14177.
37 I. Gutiérrez, E. Diaz and S. Ordóñez, *Thermochim. Acta*, 2013, **567**, 79–84.
38 H. Chen, L. F. Wang, J. Yang and R. T. Yang, *J. Phys. Chem. C*, 2013, **117**, 7565–7576.
39 L. F. Wang, N. R. Stuckert, H. Chen and R. T. Yang, *J. Phys. Chem. C*, 2011, **115**, 4793–4799.
40 C. Zlotea, R. Campesi, F. Cuevas, E. Leroy, P. Dibandjo, C. Volkringer, T. Loiseau, G. Férey and M. Latroche, *J. Am. Chem. Soc.*, 2010, **132**, 2991–2997.
41 S. Proch, J. Herrmannsdorfer, R. Kempe, C. Kern, A. Jess, L. Seyfarth and J. Senker, *Chem.–Eur. J.*, 2008, **14**, 8204–8212.
42 M. Sabo, A. Henschel, H. Fröde, E. Klemm and S. Kaskel, *J. Mater. Chem.*, 2007, **17**, 3827–3832.
43 X. M. Liu, S. Rather, Q. X. Li, A. Lueking, Y. G. Zhao and J. Li, *J. Phys. Chem. C*, 2012, **116**, 3477–3485.
44 S. Y. Lee and S. J. Park, *Int. J. Hydrogen Energy*, 2011, **36**, 8381–8387.
45 S. J. Yang, J. H. Cho, K. S. Nahm and C. R. Park, *Int. J. Hydrogen Energy*, 2010, **35**, 13062–13067.
46 L. F. Wang, A. J. Lachawiec Jr and R. T. Yang, *RSC Adv.*, 2013, **3**, 23935–23952.
47 T. Y. Wang, Q. J. Zhang, B. H. Li, H. Chen and L. Chen, *Int. J. Hydrogen Energy*, 2012, **37**, 5081–5089.
48 M. A. Miller, C. Y. Wang and G. N. Merill, *J. Phys. Chem. C*, 2009, **113**, 3222–3231.
49 Z. Wang and R. T. Yang, *J. Phys. Chem. C*, 2010, **114**, 5956–5963.